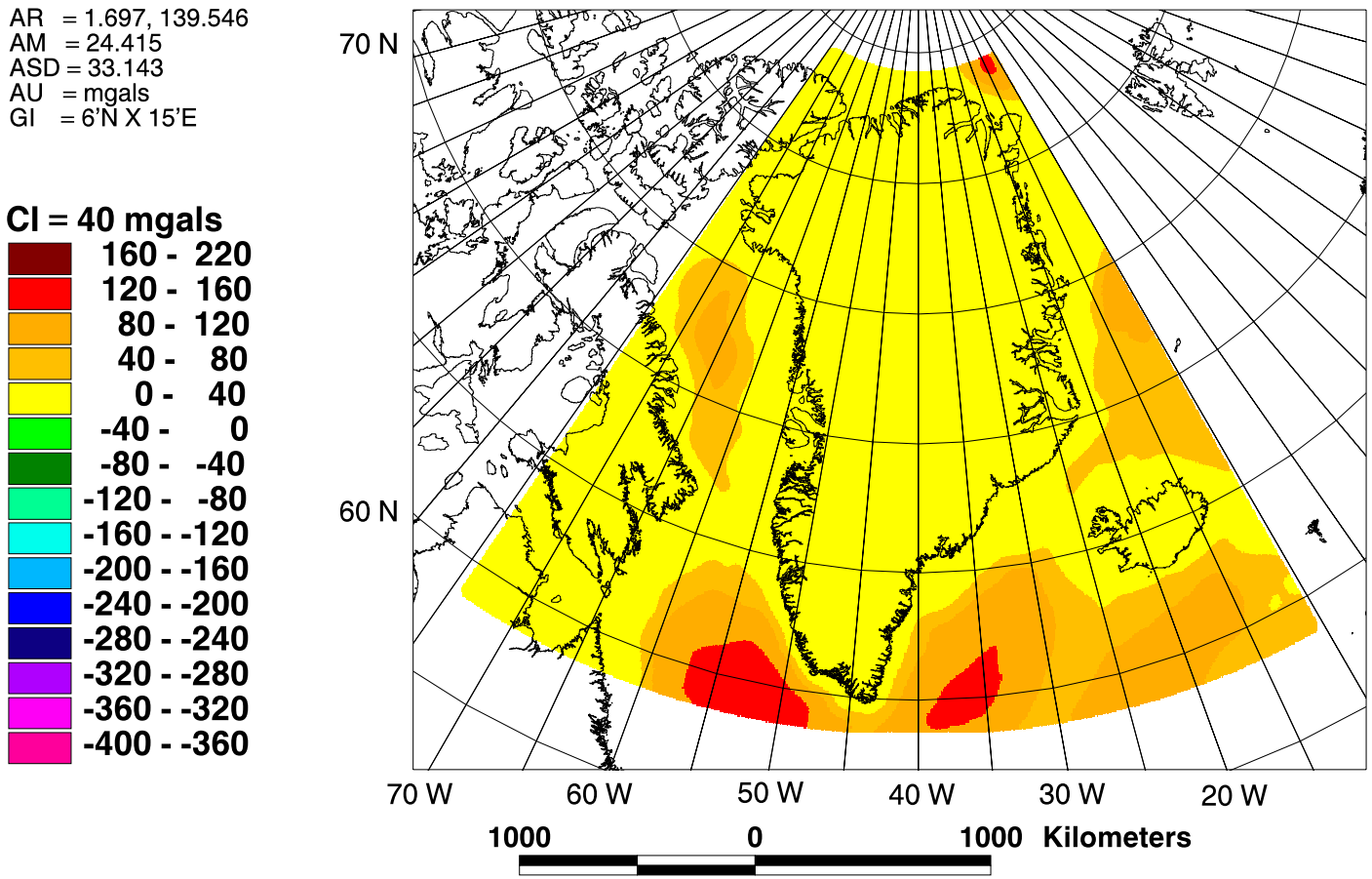

Figure 3.18: Gravity effect of the ocean model at 20-km above MSL in a Lambert Equal-Area Azimuthal Projection centered on 40° W.

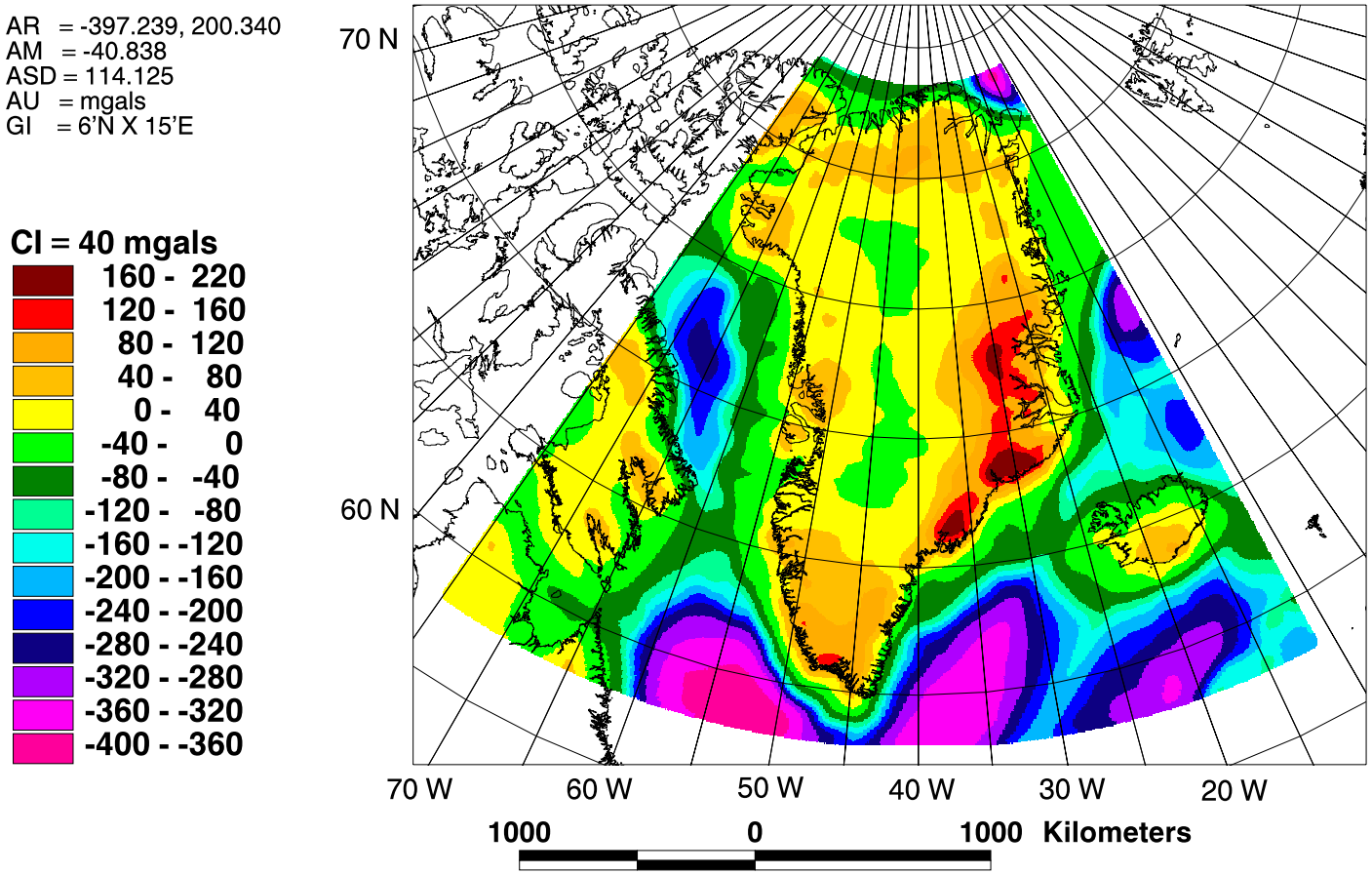

Figure 3.19: Gravity effect of the rock model at 20-km above MSL in a Lambert Equal-Area Azimuthal Projection centered on 40° W.

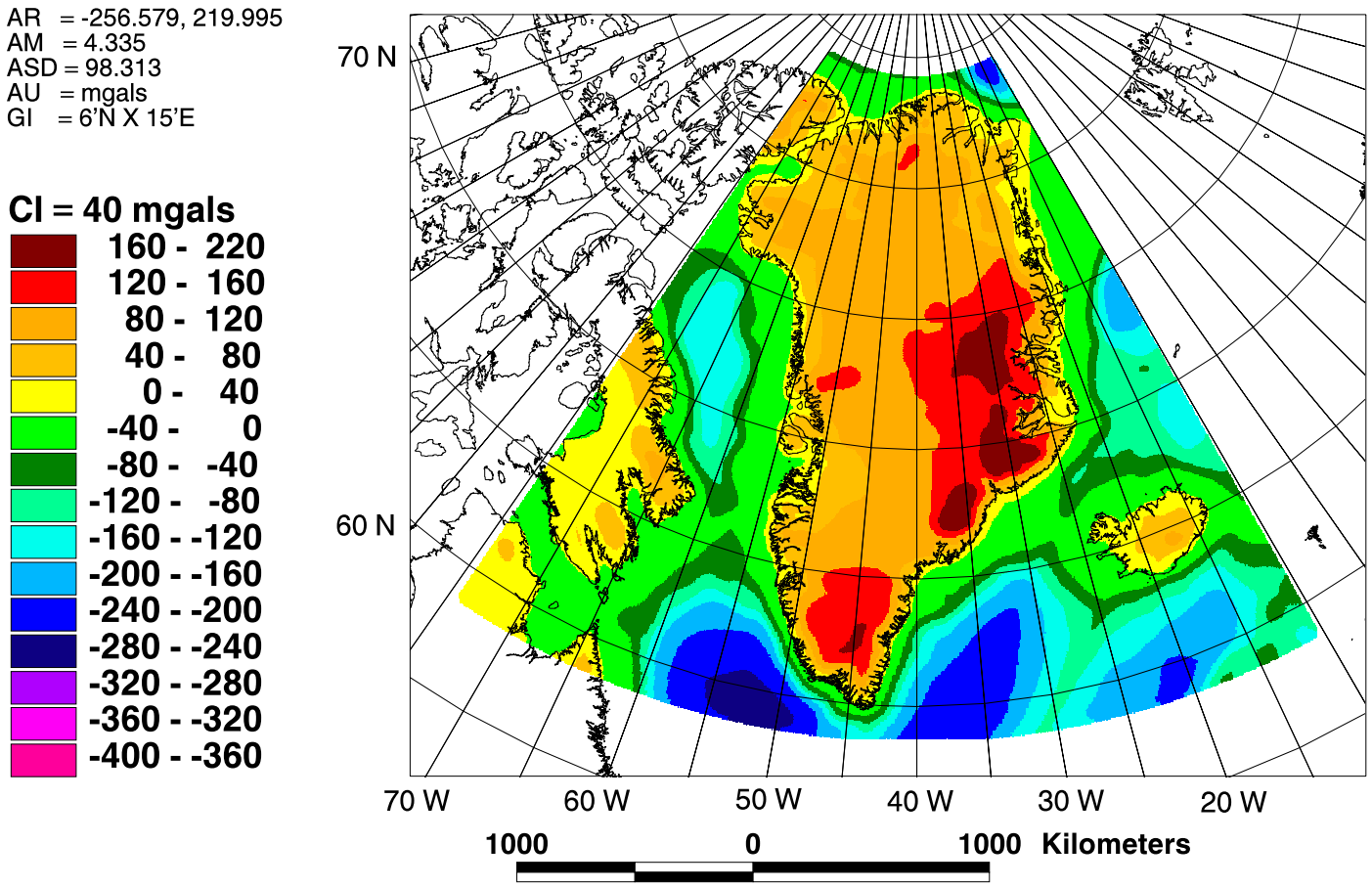

Figure 3.20: Terrain gravity effect (TGE) from the summation of the gravity effects of the ice, ocean and rock models at 20-km above MSL in a Lambert Equal-Area Azimuthal Projection centered on 40° W.

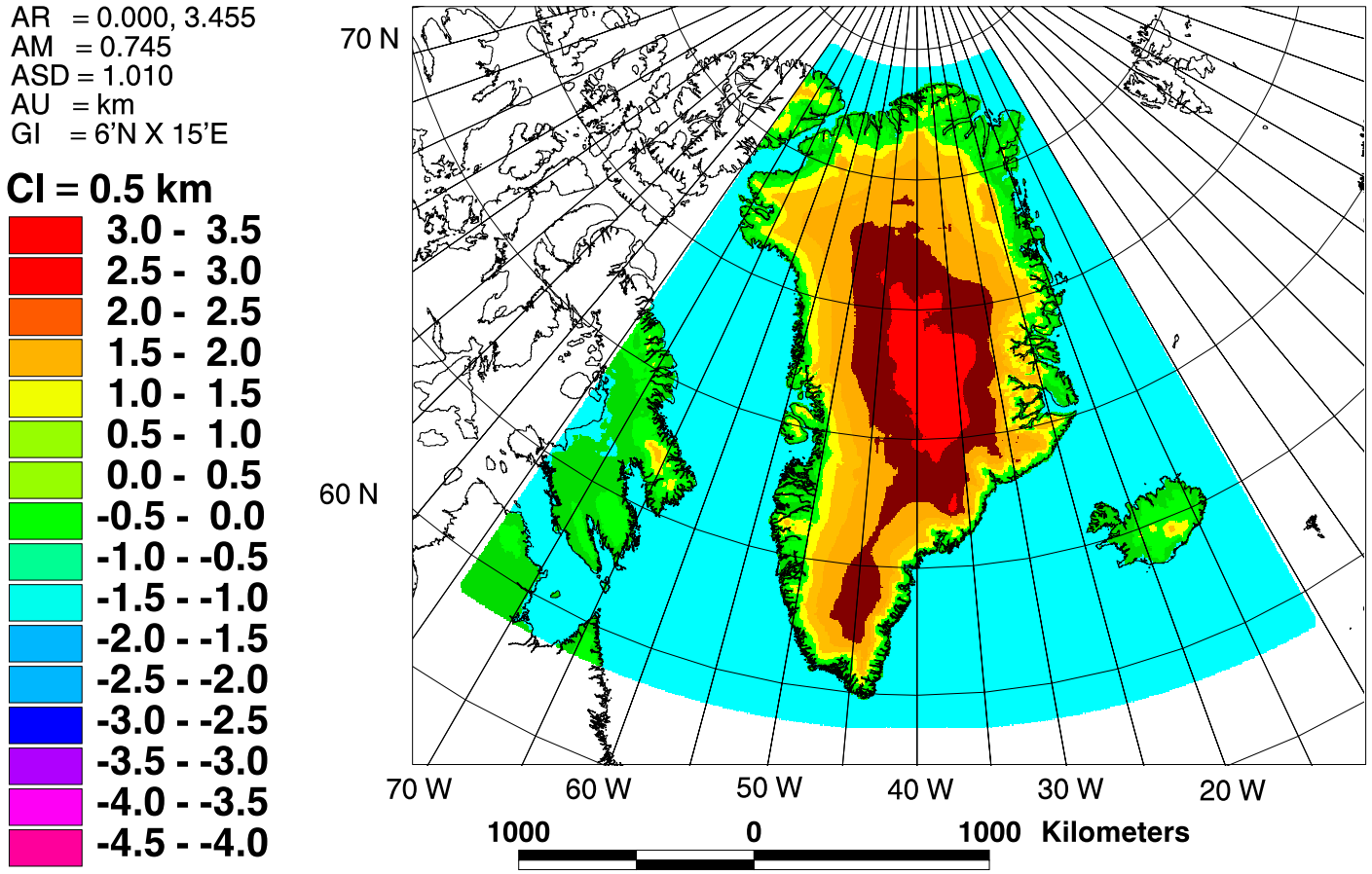

Figure 3.21: Total of three terrain models (the Earth's surface) in a Lambert Equal-Area Azimuthal Projection centered on 40° W (reference is MSL). Elevations on Greenland are from Ekholm [1996] (Figure 3.1), ocean areas are zero (MSL), and all other terrestrial areas are from JGP95E (Figure 3.6).

By these efforts, the initially low correlation between the TGE and the FAGA (CC=0.12) was reduced to zero in the terrain decorrelated subset of the FAGA (i.e., TDFAGA) data that are shown in Figure 3.23. Removing TDFAGA from the FAGA generated the terrain correlated subset of the FAGA (i.e., TCFAGA) data given in Figure 3.22. Consideration of the standard deviations of TDFAGA and TCFAGA suggest that they each have about half the energy of the FAGA.

Assuming Airy isostatic compensation, regions either under- or over-compensated will have isostatic anomalies that are a function of the relief and with effects that will be incorporated into the FAGA. The components of the FAGA that are most related to the varying terrain are given by TCFAGA. Conversely, TDFAGA reflect all other elements that comprise the FAGA, such as lateral density variations in the crust, mantle and core, and errors in the data and assumptions, etc.

Removing TCFAGA from the TGE provides an estimate of the compensated TGE (CTGE), which represents the gravity effects of the three terrain types under crustal equilibrium. This approach is feasible because 90% of the earth is in equilibrium with the mean global gravity anomaly being zero [Heiskanen and Moritz, 1967]. Therefore, regions that have correlative relationships between the crust and FAGA may reflect imbalances in compensation. The degree of isostatic imbalance would directly reflect the magnitude of the correlative FAGA. Hence, removing the components of FAGA related to terrain (TCFAGA) dampens the effect of disequilibrium in TGE.

The global average FAGA signal being zero requires that the gravity signal implied by the compensated crust (CTGE) have an annihilating counterpart (ACTGE) as shown in Figure 3.24. A possible way to account for these ACTGE is by the density contrast between the crust and the mantle across the Moho boundary. By linearizing the physical relationship between the ACTGE and the mass variations implied by

the Moho undulation, the Moho depths may be estimated using the least squares inversion discussed in the methodology section (Equation 3.5).

Unfortunately, the difficulties with this approach revolve around the size of the design matrix and its inversion. This field area consists of a 256 by 256 set of unknowns being derived from a 256 by 256 set of observations. This requires a 65536 by 65536 design matrix because all elements are related. Just to generate the design matrix, required data storage (34 Gb) and processing time (42 days) far exceed those currently available on the Ohio Supercomputer platforms. Use of out-of-core solutions is currently being explored, but this remains an area that is little understood even by Cray personnel.

Due primarily to storage and processing difficulties, this approach could not be attempted for the full solution. Instead a simplifying assumption that the ACTGE at a single observation point can be attributed entirely to mass anomaly (depth of root) at the nadir point in the Moho depth model. This relationship is expressed by reordering the components in the Bouguer Slab approximation given in Equation 3.9 to:

$$h_{root} = \frac{g}{2\pi G \Delta\rho} \tag{3.10}$$

where: h_{root} = root depth below mean reference depth;
g = gravity value from the ACTGE grid;
$\Delta\rho$ = density contrast between the mantle and lower crust; and
G = gravitational constant = 6.672 mgals/[(gm/cm^3)*km]

This approach requires more iterations and permits only a poor constraint with available seismic depth data. Long wavelength aspects of the seismic data were incorporated into an early iteration to reduce the number of iterations required to generate closure. This simplified relationship permits rapid calculations of the Moho depths for each iteration but requires more iterations to account for its inherent assumptions.

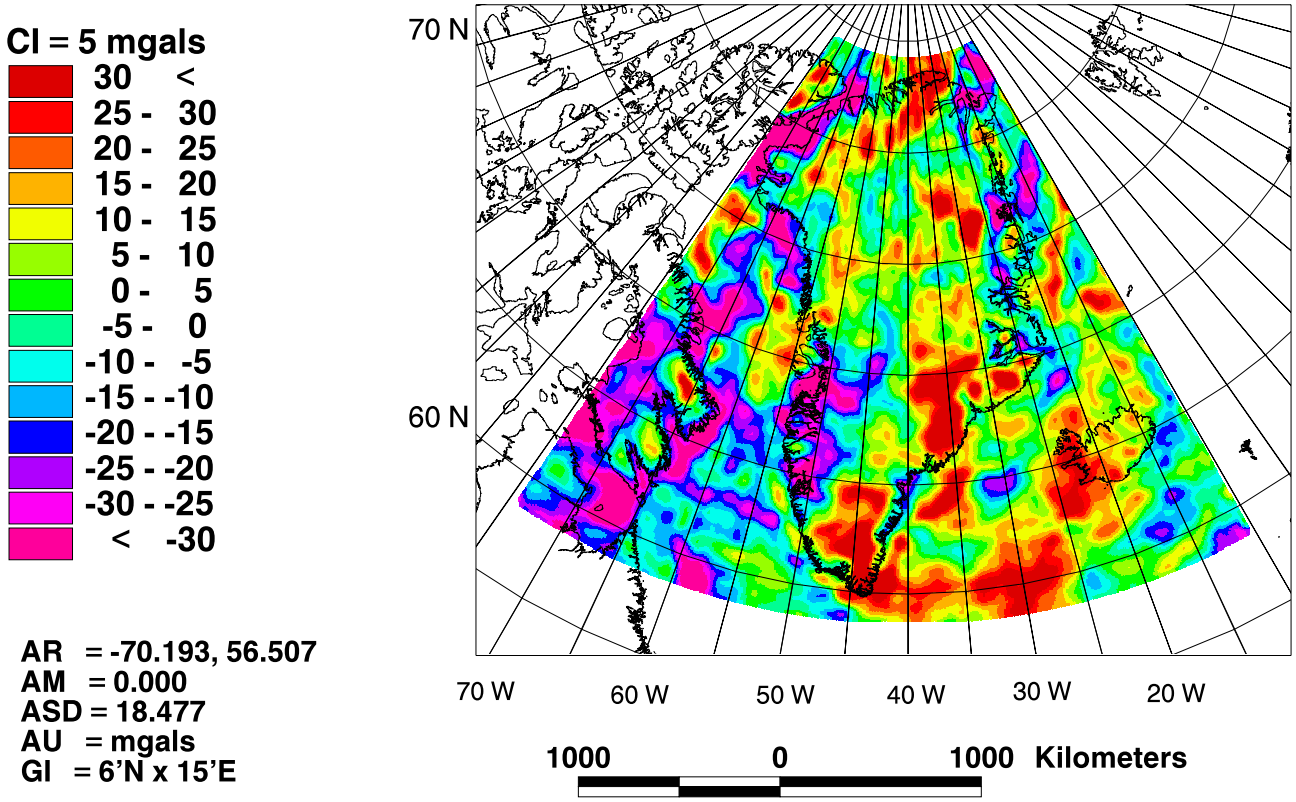

Figure 3.22: Terrain Correlated FAGA (TCFAGA) in a Lambert Equal-Area Azimuthal Projection centered on 40° W at 20-km above MSL. These data represent that component of the reference FAGA that show the highest positive and negative correlations with the TGE.

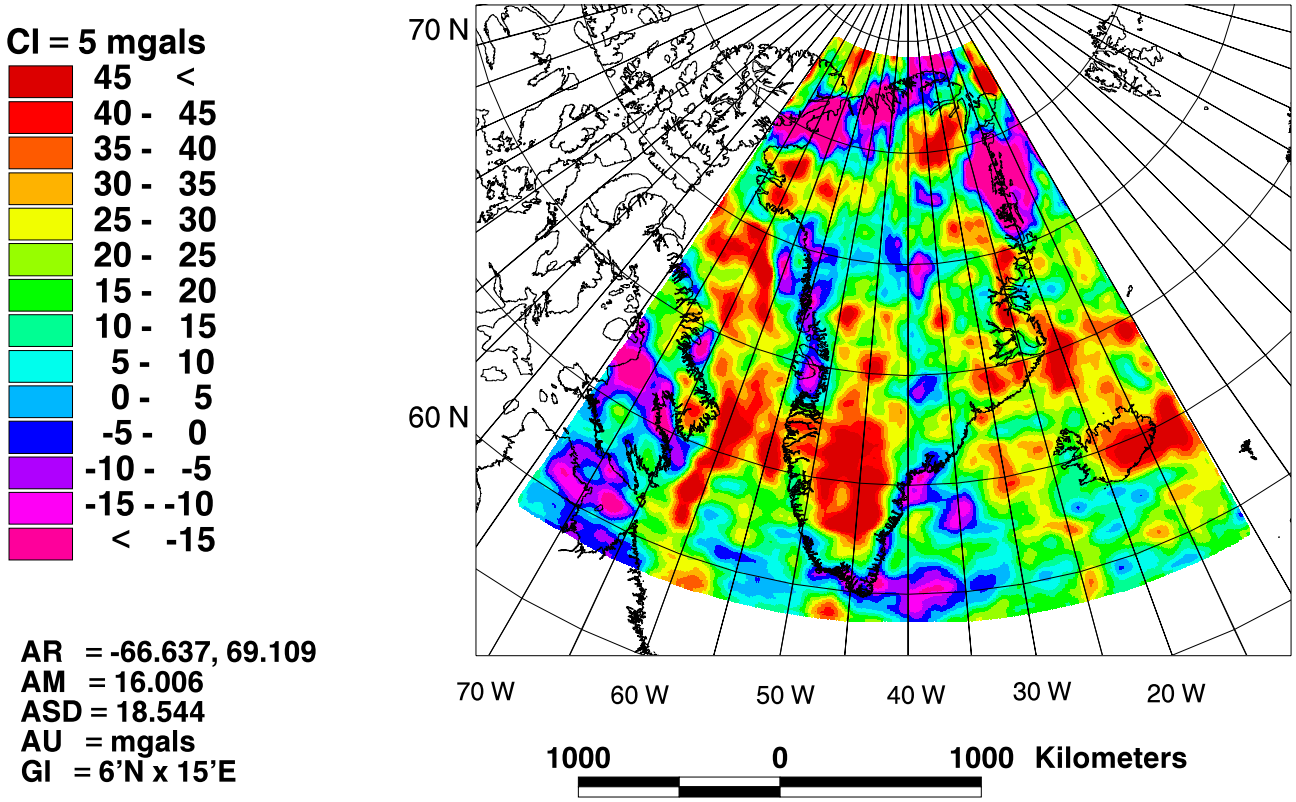

Figure 3.23: Terrain Decorrelated FAGA (TDFAGA) in a Lambert Equal-Area Azimuthal Projection centered on 40° W at 20-km above MSL. These data represent that component of the reference FAGA that is left over after removal of TCFAGA.

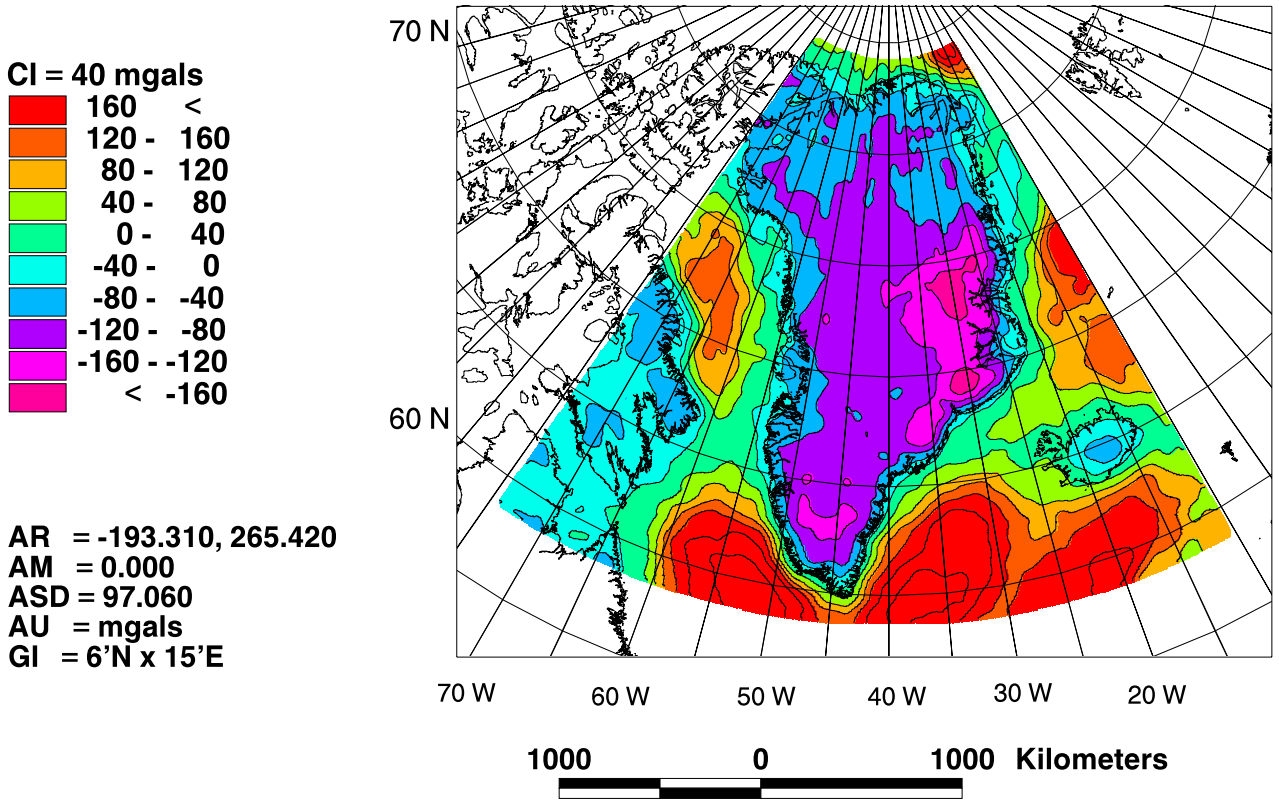

Figure 3.24: Annihilating CTGE (ACTGE) in a Lambert Equal-Area Azimuthal Projection centered on 40° W at 20-km above MSL. These data represent the gravity effect of the Moho undulation based upon an assumed density contrast.

GLQ integration (Equation 3.1) is employed to determine the RGE of the initial Moho depth model. The RGE is removed from the ACTGE to generate a residual ACTGE that is then used to generate a modification to the initial Moho depths. Using the initial lower crustal density assumptions (Figure 3.16), approximately 12 iterations were required to generate the best-fit Moho depth model shown in Figure 3.25.

The RGE generated using the Moho depth model with the initial lower crustal density values compared favorably with the ACTGE (CC=0.96). To further reduce the residual ACTGE, the Moho depths were fixed and the density contrasts were adjusted using a Bouguer slab approximation:

$$\Delta\rho = \frac{g}{2\pi G h_{root}} \tag{3.11}$$

The density contrasts at the Moho boundary were iterative solved using a similar procedure whereby residual ACTGE values were used to further adjust the density contrasts. After about 5 iterations, the residual ACTGE showed no further decrease and the adjusted lower crustal density contrasts are given in Figure 3.26. When these density contrasts are used in a GLQ calculation with the Moho depth model (Figure 3.25), the resulting RGE, given in Figure 3.27, showed better agreement with the ACTGE (CC=0.97). The final residual ACTGE was reduced from 27 mgals to 24 mgals and is shown in Figure 3.28. It shows that most of the remaining unmodeled effects are constrained along the eastern and southern sides of the grid. This is consistent with edge effects derived from the iterative process and will not be explored further.

The ACTGE field is modeled almost completely (96%) by the Moho depths with only about 1% being modeled by the lateral density variations. With the predictions for a final Moho depth model complete, these values may be compared to the seismic depth estimates and examined for implied geologic structure.

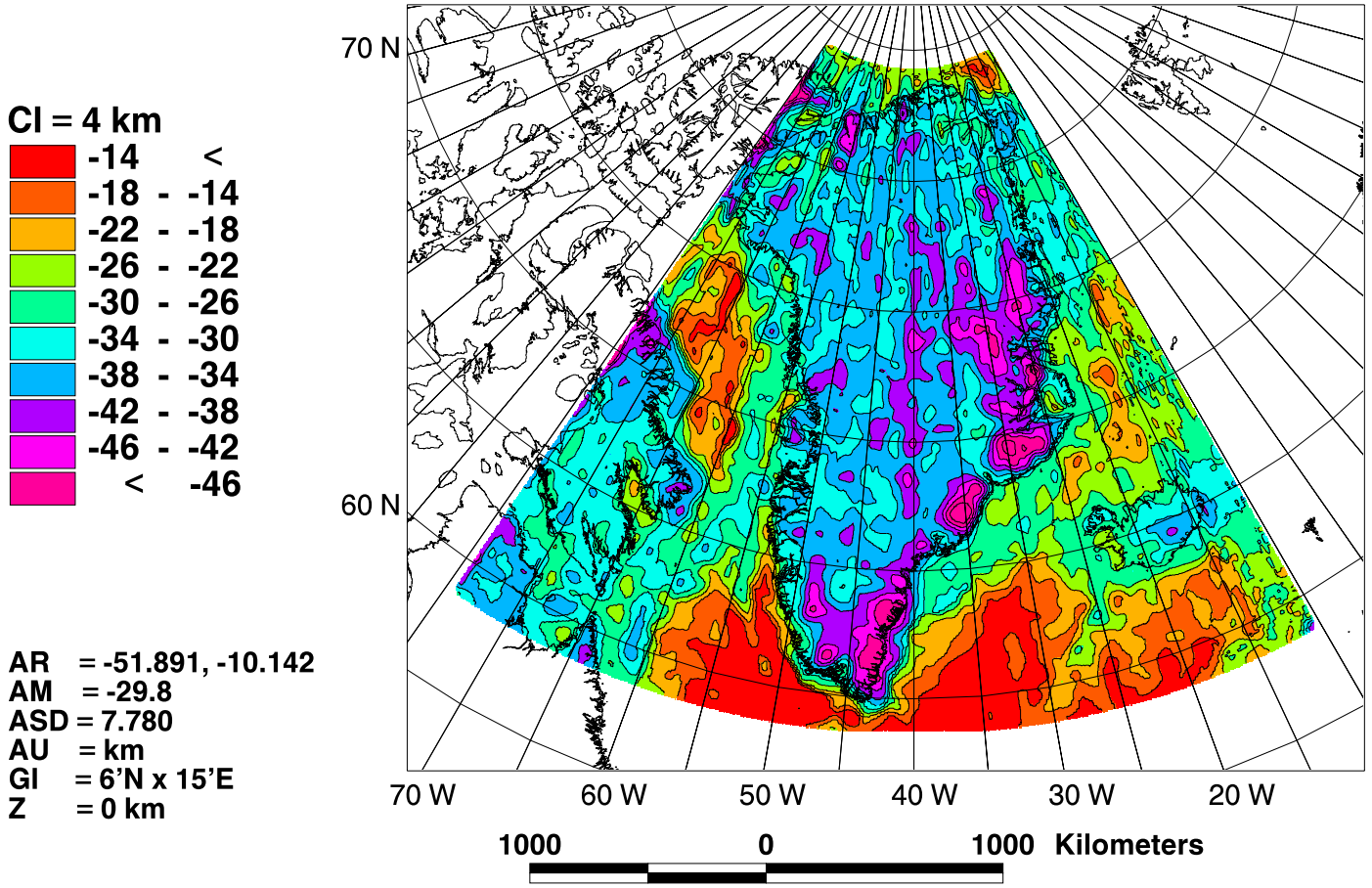

Figure 3.25: Moho depth model for the Greenland study area in a Lambert Equal-Area Azimuthal Projection centered on 40° W. This model was calculated iteratively using the initial assumed densities for the lower crust shown in Figure 3.16 and the simplified relationship given in Equation 3.10.

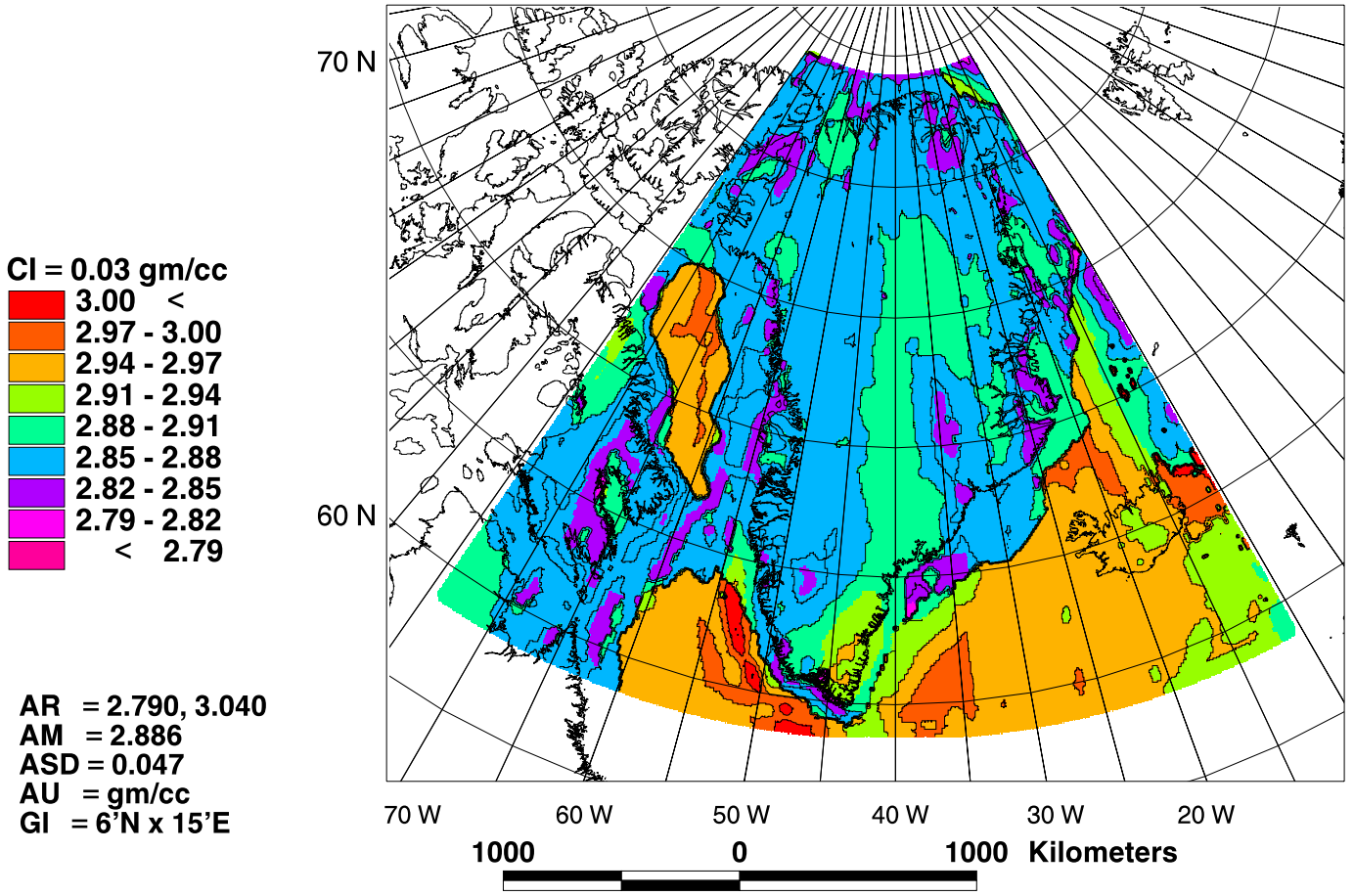

Figure 3.26: Adjusted density model for the Greenland field area in a Lambert Equal-Area Azimuthal Projection centered on 40° W. These values were determined by fixing the Moho depths to those determined for Figure 3.25 and modifying the initial assumed densities (Figure 3.16) to iteratively solve Equation 3.11.

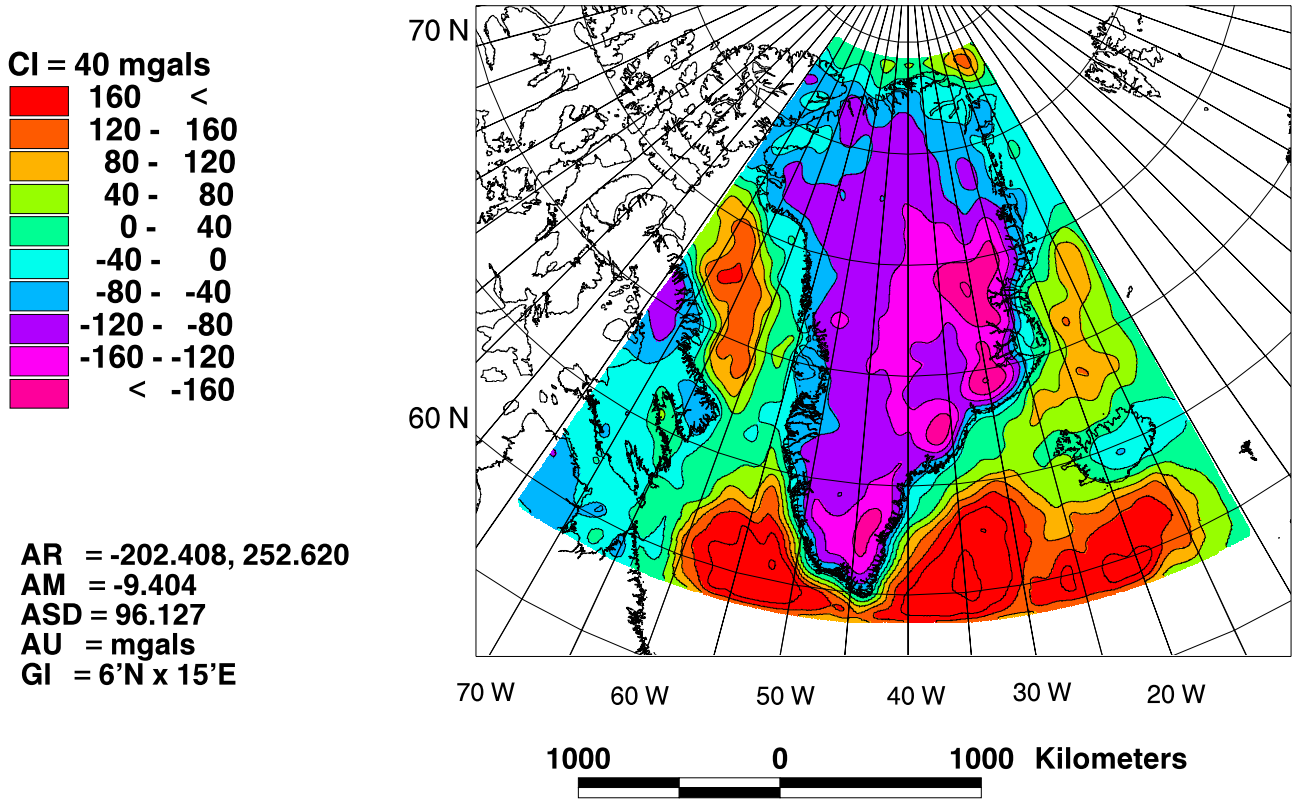

Figure 3.27: Root Gravity Effect for Greenland derived from the Moho depth model (Figure 3.25) and adjusted lower crustal density contrasts (Figure 3.26) in a Lambert Equal-Area Azimuthal Projection centered on 40° W.

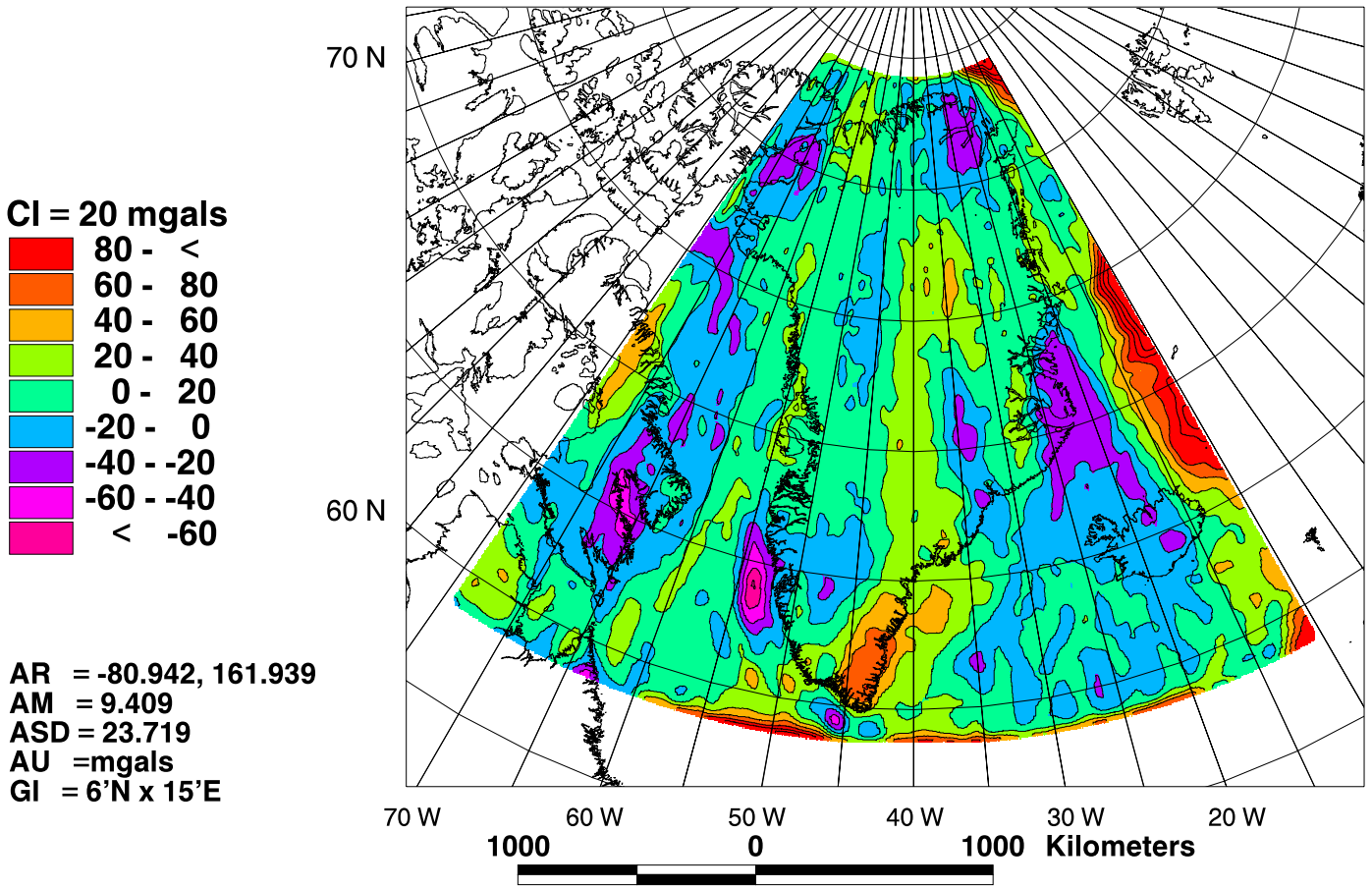

Figure 3.28: Unmodeled residual ACTGE for Greenland in a Lambert Equal-Area Azimuthal Projection centered on 40° W. These data represent the difference between the ACTGE (Figure 3.24) and the RGE (Figure 3.27) calculated from the Moho depths and adjusted densities. Remaining unmodeled effects are dominantly located along the southern and eastern edges of the field area that probably represent edge effects.

3.7 Comparisons with Other Available Moho Depth Estimates

In an effort to assess the quality of the Moho depth grid, it was interpolated to the locations where seismically determined Moho depth estimates were available. These points are statistically examined to determine the amount of agreement.

Additionally, the BPRC profile data are used to generate an approximation of the Moho depths assuming an Airy model of compensation. This model is compared to interpolated values from Figure 3.25 only to determine if their are major areas of disagreement. The Moho depth profile generated by the BPRC data will not sufficiently take into account off axis features but should account for most regional features.

3.7.1 Comparison with Seismic Moho Depth Estimates

Depths interpolated from the Moho depth grid (Figure 3.25) were next compared with available seismic depths from 7 profiles. Although these seismic depth estimates were also used in the determination of the Moho depth model, they are evaluated here because

The first profile starts over oceanic bedrock passes over transitional crust and onto continental crust [Chian and Louden, 1994]. The second profile [Chian and Louden, 1992] parallels the coast over continental crust. The third profile [Dahl-Jensen et al., 1998] is over oceanic crust offshore southeastern Greenland. The fourth profile [Fechner and Jokat, 1996] is over continental crust in the Scoresby Sund. The data from Gregersen et al. [1988] is actually a series of distant points. The sixth profile [Jackson and Reid, 1994] and the seventh profile [Reid and Jackson, 1997] are over northern Baffin Bay in a region that is partially oceanic, transitional, and continental crust.

Since no error estimates were available for the seismic data, they cannot be definitively used to assess the errors in the Moho depth model. It was assumed that sufficient statistical agreement between the seismic estimates and those from the model would mean that both data sets are valid and that points in disagreement would be rejected from the statistical analysis. As a criteria for determining agreement, $\pm 2\sigma$ of the RMS difference was selected because most (95%) data should fall into this interval.

Thirty-nine seismically-determined Moho depth estimates occurred within the field area along these 7 profiles. If no data are removed, then the 39 points correlate at 0.89 (calculated in accordance with Davis [1986]), the numeric RMS difference was 4.6 km, and the mean numeric difference was 0.1 km. To make the error estimate dimensionless and to indicate the proportion of the error, a percent difference was determined at each point by dividing the numeric difference by the seismic Moho depth estimate. Using all percent differences, the percent RMS difference was 18.3% for all 39 points.

Six of these points fell outside the $\pm 2\sigma$ criteria for either the RMS difference or the percent RMS difference. Removal of these 6 points increases the CC to 0.95, reduces the numeric RMS difference to 3.4 km, increases the mean numeric difference only to 0.4 km, and reduces the percent RMS difference to 13.1%. This indicates that interpolated Moho depth values conformed generally to about 86.9% of the seismic reference depths (further details of this analysis are given in Appendix E).

The mean depth of 30.0 km used in this study was based upon the results of the comparison with the seismic data. The Moho depth prediction grid was interpolated to the seismic depth locations, and these values compared with the seismic depths. If the average of the interpolated depths from the initial simplified inversion was deeper than the average of the seismic depths, then the reference surface was made shallower.

This process continued with subsequent iterations until 30.0 km was determined to be the best reference depth to use during the GLQ calculation of the RGE.

3.7.2 Comparison of Interpolated and BPRC Profile Moho Depth Data

To check the quality of the Moho depth grid (Figure 3.25), a Moho depth profile was generated along the BPRC survey from data presented in Appendix D (Figure 3.11). An Airy model [Heiskanen and Moritz, 1967] of local isostatic compensation was selected to be consistent with that used for the Moho depth grid (Figure 3.25). However, the profile will not properly estimate features due to sources located off-axis. Hence, the comparison is only intended to show a general agreement.

The Ekholm ice surface [Ekholm, 1996] and subglacial elevation [Sohn and Csathó, 1998; Gudmandsen, 1970] data were used to model the Moho boundary as generalized in Figure 3.29. Assuming that the region is already in isostatic compensation and that ice thickness estimates are reliable, the depth to the Moho may be estimated from the terrain profiles by:

$$h_{root} = \frac{\rho_{ice} \cdot \Delta h_{ice} + \rho_{uc} \cdot h_{rk/ic}}{\rho_m - \rho_{lc}} + T, \tag{3.12}$$

where: h_{root} = root depth
ρ_{ice} = ice density = 0.90 gm/cm^3
Δh_{ice} = ice thickness (top minus bottom of ice sheet elevations)
ρ_{uc} = upper crustal density = 2.74 gm/cm^3
$h_{rk/ic}$ = elevation of rock/ice boundary above/below reference ellipsoid
ρ_m = mantle density = 3.30 gm/cm^3
ρ_{lc} = lower crustal density = 2.86 gm/cm^3
T = average crustal thickness = 30 km

The same crustal and ice densities used to determine the Moho depths of Figure 3.25 by GLQ integration were also used to estimate the Moho depths by Equation 3.12 along the BPRC profile shown in Figure 3.11. Moho depth estimates from Figure 3.25 were interpolated at the profile locations and compared in Figure 3.30.

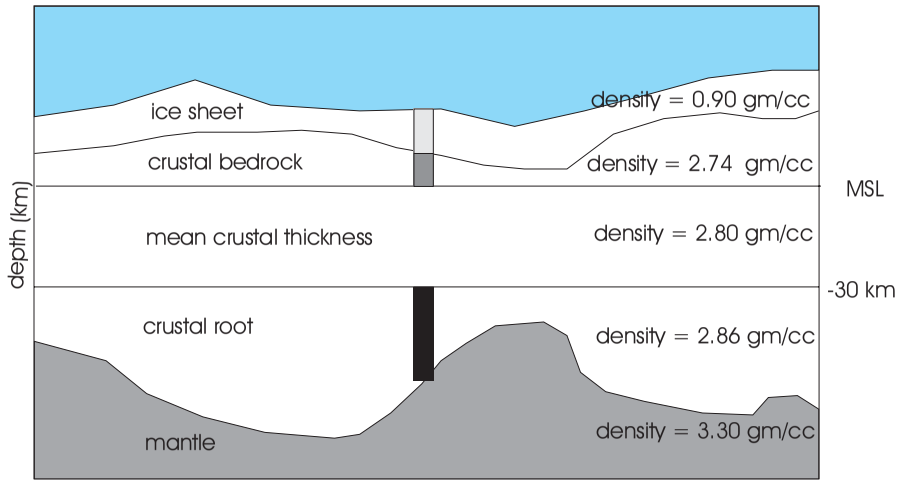

Figure 3.29: Generalized depiction of Moho depth profile generation by Equation 3.12. The ice sheet is shown on top of the subglacial bedrock, which sits on top of 30 km of crust. Beneath this extends the crustal root into the mantle. The masses in the top two boxes (for ice and subglacial bedrock) must equal the mass in the bottom box (in the root) to agree with the assumed Airy method of isostatic compensation.

The interpolated and profile Moho depth data are fairly similar (CC = 0.57) and have little mean difference (0.20-km). However, their RMS difference (3.47 km) is more significant and may reflect differences in the underpinning assumptions used to derive the profile, such as not taking into account the spherical geometry of the problem and assuming that the region is already in isostatic equilibrium. However, this RMS difference is consistent with the RMS difference between the Moho depth model and the seismic Moho depths (3.4 km).

For the most part, the two sets of predictions are fairly consistent. There appears to be a long wavelength (3000 km) component to the differences in Figure 3.30.b that is overlain by a higher frequency components. The most significant minima occur near the 2000 and 4000 km points in the profiles, possibly originating near thin spots in the ice cover. The trend in the differences mirrors the root topography, hence

it is assumed that the BPRC-profile Moho depth estimates are under-predicting the interpolated Moho depth values.

The Moho depths (Figure 3.25), best-fit lower-crustal density contrasts (Figure 3.26), and residual ACTGE (Figure 3.28) highlight unique features about the crustal structure around Greenland. These features will now be examined, especially in the context of seismic surveys that have sampled the crust throughout the field area.

3.8 Discussion

The Moho depths shown in Figure 3.25, best-fit lower-crustal densities shown in Figure 3.26, and residual ACTGE shown in Figure 3.28 highlight unique features about the crustal structure around Greenland. The features present in the Figures 3.26 and 3.28 might point to regions where this assumption is invalid, the location of transitional crust, dynamically supported regions, or regions where results might be suspect.

The adjusted lower-crustal densities shown in Figure 3.26 clearly show the selected 1 km depth contour where the initial assumed densities were differentiated between oceanic and continental rock. Although this hampers determination of the transitional crust location, other features are present that might indicate the extent of the geologic structure. The adjusted densities indicate primarily a long wavelength trend across the region with some shorter wavelength features along the southwestern Greenland coast into the Davis Strait and Baffin Bay. The residual ACTGE contain more short to intermediate wavelength signal, but this is primarily due to edge effects from processing along the southern and eastern edges of the field area.

Regionally, the Moho depth map shown in Figure 3.25 shows the most expression when compared to the best-fit lower-crustal densities shown in Figure 3.26 and the

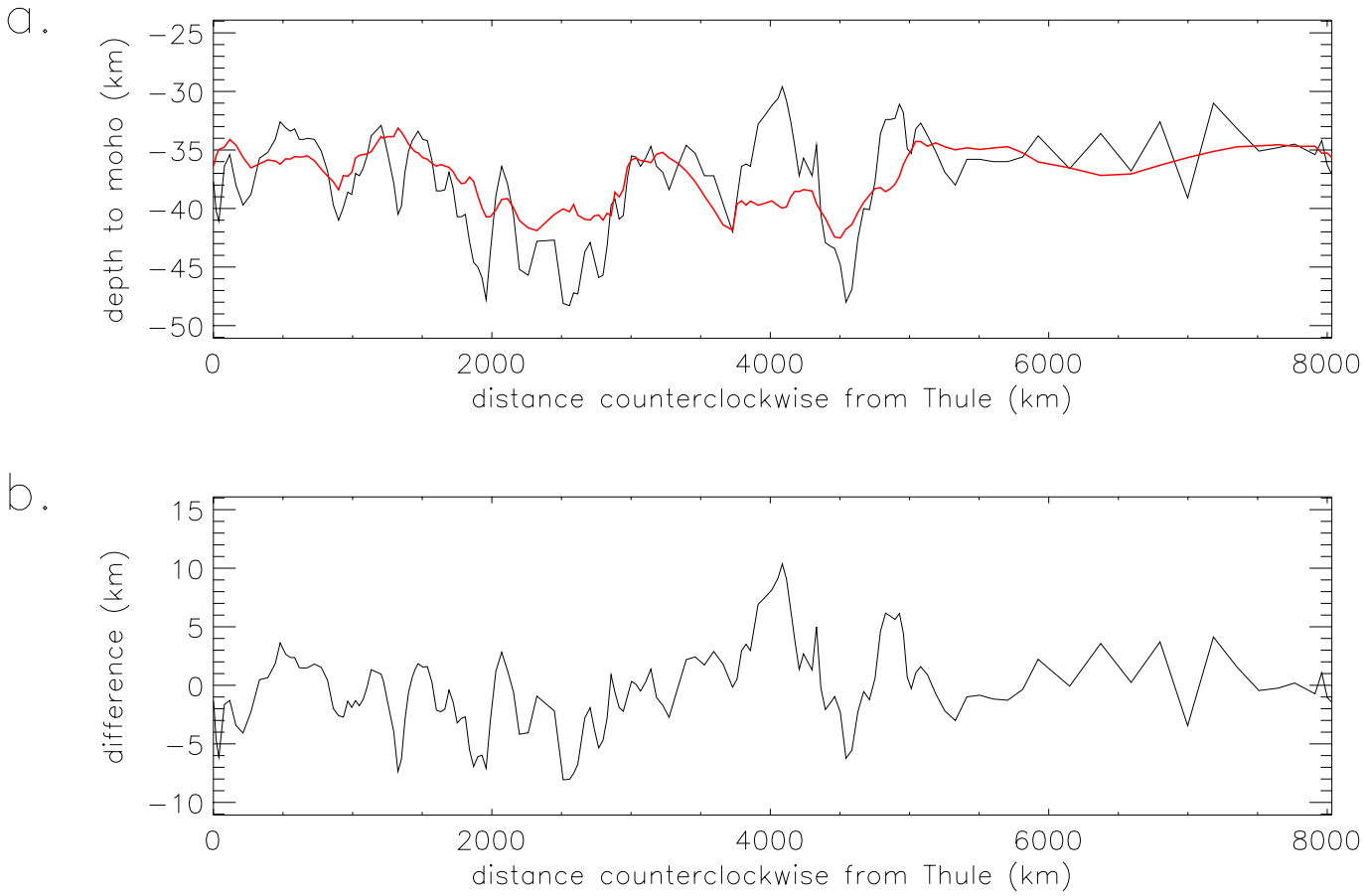

Figure 3.30: Cross-section of interpolated and profile Moho depth data. **a.** Values from the Moho depth grid (Figure 3.25) were interpolated to the locations of a Moho depth profile (thick-red). The profile was determined from the ice surface and subglacial models as shown in Figure 3.29 and given in Equation 3.12 assuming an Airy method of compensation. **b.** Plot of the difference (interpolated - profile).

residual ACTGE shown in Figure 3.28. This is because of the first order assumption that density contrasts created by Moho depth variations generated the ACTGE signal. These features will now be examined, especially in the context of seismic surveys that have sampled the crust throughout the field area. This discussion will start on features located or inferred in southern Greenland proceeding clockwise and finishing in the central regions.

At the very southern tip of Greenland, an apparent right-lateral transform fault can be seen to offset a region of deeper crust away from the coastline. This location is consistent with the Julianhaab Fracture Zone shown in a geologic map of Greenland produced by Escher and Pulvertaft [1995]. The oceanic crust produced in this fracture zone is not assigned to a magnetic isochron by Escher and Pulvertaft [1995], but it is ascribed to isochrons 27 or older (63 Ma) by Roest & Srivastava [1989] and Srivastava & Roest [1995].

Another area described by Srivastava and Roest [1995] as oceanic occurs along the Labrador Sea margin of Greenland. They attributed an oceanic origin based on coast-parallel magnetic features, which they determined to contain magnetic lineations complete through isochron 33 starting at about the 1 km isobath.

Anomalous features in Figure 3.25) indicate deeper roots extending sub-parallel to the southwestern Greenland coastline, which do not agree with previous magnetic interpretations [Roest and Srivastava, 1989; Srivastava and Roest, 1995]. The transition perpendicular to the coastline is then from very deep roots under southwestern Greenland, to very shallow roots immediately offshore, to the deeper coastal sub-parallel roots mention above, and then to shallow roots in the oceanic areas of the Labrador Sea. A Moho depth profile generated by a seismic survey over this same region [Chian and Louden, 1992; 1994; Chian et al., 1995a; 1995b] suggested similar results and divided the crust into zones of continental, transitional, and oceanic crust.

The transitional crust described by Chian and Louden [1994] contained a possible serpentinized mantle diapir in the deeper root and shallow seated mantle adjacent to that. Because both features originated from mantle rocks, they both would have higher densities with the density of the mantle diapir expected to be lower due to the serpentinization. The distinctness of transitional and oceanic crust is clear in Figure 3.26 where a band of higher density (> 3.00 gm/cm^3) crust lies just offshore of southwestern Greenland with a spoon-shaped zone of less dense (2.95 gm/cm^3) crust further offshore.

The transitional crustal zone of Chian and Louden [1994] encompasses the regions of very shallow roots immediately offshore and the deeper coastal sub-parallel roots. Hence the crust in this region will be categorized by 4 zones consisting of 1) continental, 2) rifted-continental, 3) transitional, and 4) oceanic crust.

The continental crust (zone 1) has normal continental crust densities ($\sim$2.85 gm/cm^3), very deep roots, and encompasses the region of southwestern Greenland out to the 1 km isobath in Figure 3.25. The rifted-continental crust (zone 2) has higher density values than is typical for oceanic crust (> 3.00 gm/cm^3), very shallow roots, and its extents are defined by the shallow coast-parallel zone in Figure 3.25. The transitional crust (zone 3) has densities slightly higher than is normal for oceanic crust (2.98 gm/cm^3), deeper roots, and its extent are defined by these deeper coast-parallel roots. Finally, the oceanic crust (zone 4) has typical oceanic densities (2.95 gm/cm^3), shallower roots, and occurs starting in the lobe defined by the oceanic densities in Figure 3.26.

Also supporting this interpretation, Escher and Pulvertaft [1995] noted basins of unknown origin and structure that were surrounded by oceanic crust for this same region. They also noted a wide zone of transitional crust with the oceanic crust starting at isochron 27 in about the same location as indicated by Chian and Louden

[1994]. The argument against this interpretation has been made by Srivastava and Roest [1995], because Chian and Louden [1994] do not account for the coast-parallel magnetic lineations.

These magnetic lineations may be accounted for by sea water seepage into the ruptures [O'Hanley, 1996] created by the extensive coast-parallel grabens and half-grabens described by Escher and Pulvertaft [1995] above the shallow seated mantle in the rifted-continental and transitional crust. An alternative explanation may be that the serpentinization of exhumed mantle material described by Chian and Louden [1994] as a possible source for their observed high velocity zone. This would occur further towards Greenland near the boundary between rifted-continental and transitional crust and would account for the feature described as magnetic isochron 33. Isochron 31 occurs close to the boundary of transitional and oceanic crust and would be accounted for by an extensive coast-parallel zone of serpentinized mantle material created during the rupture and initiation of oceanic spreading at about 63 Ma (isochron 27) [Brun and Beslier, 1996].

Either explanation could result in the generation of coast-parallel magnetic lineations in a region that is predominantly characterized by continental [Chalmers and Laursen, 1995] to transitional [Chian and Louden, 1994] crust. The general agreement between these models and features present in the Moho depth and adjusted density models further supports this.

Further to the north, the Davis Strait is characterized by very complicated geology [Roest, 1998] and structure (Figures 3.25 and 3.26). An area along the Greenland coast of the Davis Strait region was poorly modeled based on a significant negative residual ACTGE (-60 mgal). This is a region that is a continuation of the same coast parallel features discussed previously in the Labrador Sea. However, this region

transitions above the 1 km isobath, and the error may result from trying to model over this large discontinuity in the initial densities.

The previous coast-parallel features are much closer to the coast in this region, and the thin rifted-continental crust (zone 2) eventually disappears in the complexities of the Davis Strait. Several lower density features in the central portions of the Davis Strait appear to be related to transform faults that connected the Labrador Sea and Baffin Bay spreading centers [Roest, 1998; Okulitch, 1991].

The Baffin Bay area has shallow roots characteristic of oceanic crust (Figure 3.25) and exhibits many higher-density, shallow features along suspected spreading centers [Jackson and Reid, 1994; Reid and Jackson, 1997]. A possibly related zone of rifted-continental crust resumes north of the Davis Strait and again thins out towards the northwest.

The Nares Strait has little distinguishable in Figures 3.25 and 3.26 except for a locally shallow (28 km versus 36 km) and less dense (2.83 gm/cm^3 instead of 2.86 gm/cm^3) region beneath the Petermann Glacier. A deeper (about 40 km) feature exists under northern Greenland that appears to be an onshore extension of the Lomonosov Ridge.

The eastern coastline is complicated by the edge effects but the hotspot under Iceland and the North Atlantic spreading centers surrounding it are clear in Figure 3.25. Also in the southeastern corner of Figure 3.25, the Rockall-Hutton Bank can be seen. This bank represents the former Precambrian shelf of Greenland's southeast coast [Toft and Arkani-Hamed, 1993; Hauser et al., 1995]. The initially assigned density of 2.95 gm/cm^3 was adjusted to about 2.90 gm/cm^3 for this region and the Moho depths are estimated at deeper than 42 km, which are more typical values for lower continental crust than oceanic crust.

The Tertiary volcanic platforms in the Scoresby Sund and Blosseville Kyst regions are very distinguishable in the adjusted density model and less so in the Moho depth model. Noteworthy in Figure 3.26 is the continuation of the lower densities associated with the volcanics inland under the ice along the general path assumed for the Iceland hotspot [Morgan, 1983; Brozena, 1995; Lawver and Müller, 1994]. The regions characterized by these densities also have shallow roots (30 km) as compared to the surrounding deeper regions (50 km).

The basic structure of the South Greenland Archean province is also evident in Figure 3.25. Of particular interest is the ring-like structure in its interior. This region corresponds to the highest values in TCFAGA, which possibly mark a region that is in disequilibrium or is experiencing thermal uplift over a hotspot in the mantle. Also, all the deep roots under southeastern Greenland correspond with the region for 70 mgal errors shown in Figure 3.28. This might be another indicator that this region is in disequilibrium. Also in the southern region of Greenland, the boundary between the Ketilidian and South Greenland Archean provinces is delineated in Figure 3.26 by hook-shaped feature of 2.95 gm/cm^3 densities.

The features discussed above offer new insight into many local and regional aspects of the geologic structure of Greenland. Using the information gathered from the Moho depth map shown in Figure 3.25 and the adjusted densities shown in Figure 3.26, future research can better define the location of crustal structure and possible origins.

Finally, the Moho depth model may be differenced with the crustal rock topography model (Figure 3.5) to generate a model of the crustal thickness variations that is shown in Figure 3.31. This crustal model can be used to estimate pseudo-magnetic anomalies for comparisons with regional magnetic data and can be used to explore local to intermediate scale features for developing regional tectonic models. The

geologic structure implied by both Figures 3.25 and 3.31 can be enhanced by incorporating an analysis of the types of rocks that are located in these regions, which may be derived by comparing regional FAGA and magnetic anomaly data.

3.9 Summary

DEMs were used to determine the TGE of the various crustal components through GLQ integration. The FAGA provided by NIMA were correlated with the total TGE to find the most correlative components. These components were ascribed to regions out of isostatic equilibrium and removed from the total TGE as a means of estimating the effect of a compensated TGE (CTGE) if all regions were in equilibrium. Since the gravity effects of the CTGE are not visible in the FAGA, they are assumed to be cancelled by an annihilating CTGE (ACTGE). This gravity field may be generated by the density contrast at the Moho boundary assuming terrain is compensated by crustal thickness.

Linearized relations between the ACTGE and the Moho depth model permitted the rapid iterative calculation of a Moho depth model. GLQ integration was used to estimate the root gravity effect (RGE) of the crust based upon assumed density contrasts at the Moho boundary. This estimate was differenced with the ACTGE data, and the residuals were used to update the Moho depth model. This process was repeated until the residuals between the RGE and ACTGE could not be improved further.

The RGE of the final Moho depth model using the initial lower crustal densities correlate very strongly with the ACTGE model (CC=0.96) and have about the same power (SD = 97 mgals for both). The misfit represented by their residual was further reduced by minor adjustments of the crustal density contrasts. This step accounted

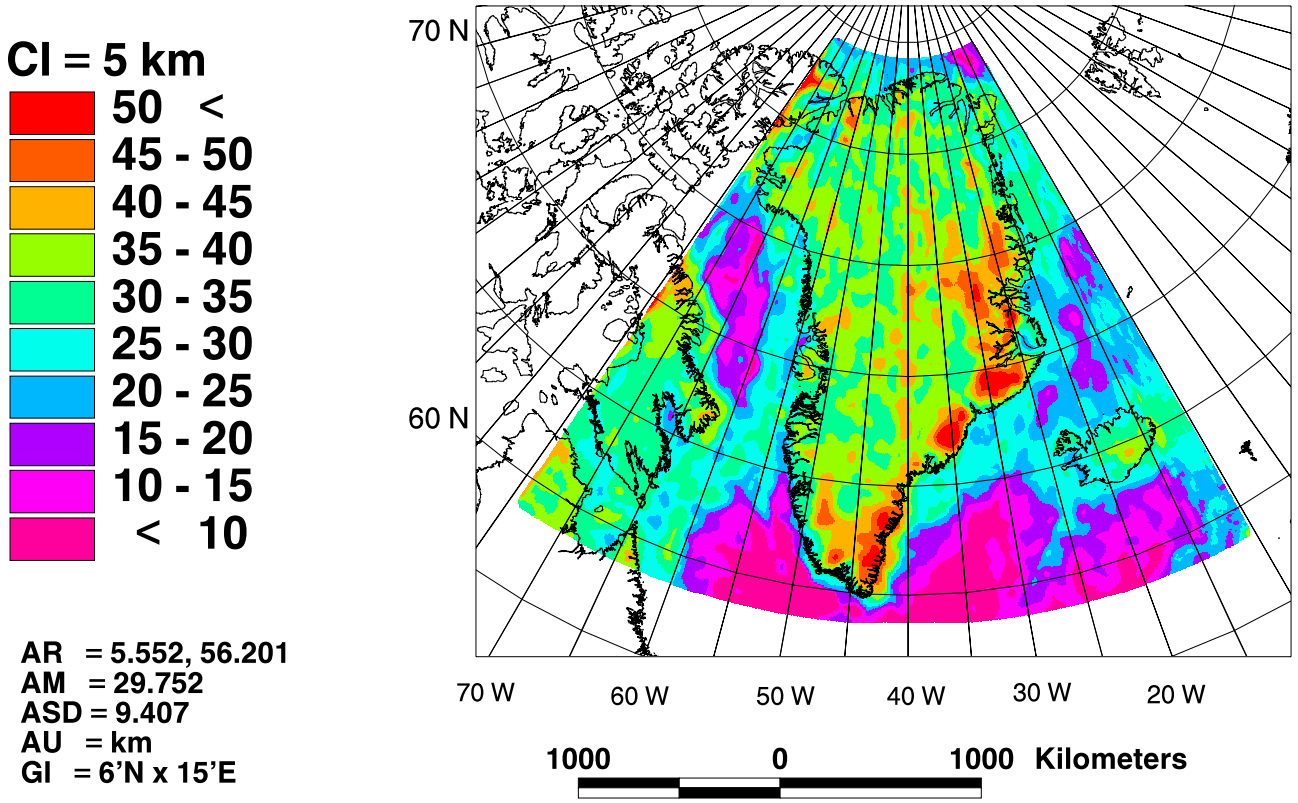

Figure 3.31: Greenland crustal thickness model derived from differencing the rock and Moho depth models in a Lambert Equal-Area Azimuthal Projection centered on 40° W.

for possible lateral density variations within the crust in accordance with the Pratt-Hayford model of isostatic compensation. The initial lower crustal densities were 2.86 gm/cm^3 and 2.95 gm/cm^3 for continental and oceanic crust, respectively. The total range of densities for the final density model varied from 2.79 to 3.04 gm/cm^3.

Both Moho boundary geometry and related density contrast contribute to the RGE. Here, the Moho boundary geometry was assumed to be the dominant factor and thus was adjusted first. The density adjustment then took care of the secondary RGE effects. The residual RGE were assumed to reflect only crustal density contrasts and not attributed to deeper sources within the Earth, as local isostatic compensation could be accommodated by the fractured crust of Greenland. After adjusting the lower crustal densities, the agreement between the RGE and the ACTGE was improved by 1% to 0.97.

The Moho depth predictions made here are on a 10 by 10 km model and may only regionally reflect the Moho undulations and, hence, may not be adequate for determining the isolated local points that are the focus of seismic soundings. Neglecting the edges, the overall standard deviation of the residual (unmodeled) ACTGE errors was about 18 mgals, which translates to $\pm$2.0 km for 95% of the data ($\pm 2\sigma$). This is consistent with the $\pm$3.4 km value derived from the 33 seismic depths. It is also consistent with the RMS difference generated during the comparison with the BPRC profile ($\pm$3.47 km).

3.10 Conclusions and Recommendations

The gravity effects of the surface terrain were modeled using Gaussian Legendre quadrature integration. These effects were modified by the removal of non-isostatic elements of free-air gravity anomalies and then used to determine Moho depths based upon an inversion of the Gaussian Legendre quadrature integration. The calculation

of this Moho depth model was constrained by seismically determined Moho depth estimates. Residual gravity effects were further modeled to determine adjusted densities for the crust in this region. The Moho depth model and adjusted densities agreed very well with crustal models based on seismic surveys.

In particular, Chian and Louden [1994] suggested that the crust off southwestern Greenland appeared to have undergone extensive crustal thinning and possible exhumation of mantle rocks during the opening of the Labrador Sea. The Moho depth model presented here is consistent with that interpretation and suggests similar variations in Moho depths occurring in an arcuate pattern sub-parallel to the coast. These features may be useful in delineating structural boundaries for future research.

Many structural and tectonic features at several different scales have been highlighted by this estimated Moho depth model. In conjunction with geologic maps, seismic surveys and magnetic data, this model of Moho depths may permit more detailed analysis of the structure and history of this region.